Research Article

Singularity-Free Adaptive Controller for Uncertain Hysteresis Suspension Using Magnetorheological Elastomer-Based Absorber

Hoa Thi Truong, Xuan Bao Nguyen ⓘ**, and Cuong Mai Bui**

The University of Danang, University of Technology and Education, Danang, Vietnam

Correspondence should be addressed to Xuan Bao Nguyen; xuanbao233@gmail.com

The magnetorheological elastomer (MRE) is a smart material widely used in recent vibration systems. A system using these materials often faces difficulties designing the controller such as unknown parameters, hysteresis state, and input constraints. First, a model is designed for the MRE-based absorber to portray the behavior of MRE and predict the appropriate electric current supplied. The conventional adaptive controller often suffers from so-called control singularities. The singularity-free adaptive controller is proposed to eliminate the singularity with parametric uncertainty. The proposed controller consists of four components: an adaptive linearizing controller, a deputy adaptive neural network controller, an auxiliary part designed for the controller to overcome the input constraint problem, and a smooth switching algorithm used to exchange the takeover rights of the two controllers. Moreover, the controller is designed to obtain the stabilization of hysteretic state estimation for the vibration system. The adaptive algorithms are proposed to update the unknown system parameters and to observe the unmeasurable hysteretic state. Meanwhile, closed-loop system stability is comprehensively assessed. Finally, the simulation performed on a quarter-car suspension with an MRE-based absorber shows the proposed controller's efficiency.

1. Introduction

Semiactive vibrating systems using magnetorheological materials have become well known. In particular, the magnetorheological elastomers (MREs) used in semiactive controls have recently emerged as a new material for vibration control [1, 2]. The system can change the natural frequency by varying the stiffness of the material. These properties are attractive for many engineering applications such as vibration isolators and vibration absorbers [3–5]. For example, Gao et al. used the MRE as a semiactive vibration isolator to suppress the vibration [4]. The results showed that the natural frequency was adjustable by 3.9 Hz. This study introduces the MRE-based absorber to reduce the suspension system's vibration caused by road irregularities and onboard engines. Using the MREs, the system can adjust its own frequency to avoid resonances for different types of road and engine speeds. It is expected that the MRE-based absorber overcomes the limitations of the MR damper. There

are many methods proposed to represent material properties in recent years [6–10]. Optimization algorithms are an effective method to determine model parameters. An innovative nonlinear model has been proposed for MRE, and an improved PSO algorithm has been designed to estimate the model's parameters [7]. An extreme machine learning method was proposed to predict the device's nonlinear (shear force) responses with applied current, displacement, and velocity level. The new swarm optimization method, called a binary coded discrete cat, was applied to select the optimal input and the number of neurons in the hidden layer for the network development [8]. The fruit fly optimization algorithm was used to determine the model parameters. A three-story standard building model under four standard earthquake excitations was tested to evaluate the model's effectiveness [9]. Artificial intelligence approaches, including linear and nonlinear regression analysis, adaptive neural fuzzy inference systems (ANFIS), and artificial neural network (ANN) techniques, are highly reliable methods for

predicting various nonlinear properties, which have been comprehensively analyzed in [10].

The MRE-based device needs a suitable controller to achieve efficiency in the vibration system. The vibration system using an MRE-based absorber is as effective as an active system without the need for large energy. In [11–15], semiactive controllers have been widely used in vibration systems, such as the sky-hook, ground-hook, fuzzy clipped on-off, and LPV approaches. These controllers do not consider the system's dynamics, so the controller does not guarantee stability in some cases. Many modern controllers have been proposed for the semiactive system, such as optimal control, adaptive control, and robust linear controller [16–18]. The adaptive control strategies ensure asymptotic stability with a small gain. However, singularities can occur, which causes a tremendous control force in these controllers. A common remedy is to limit the estimated parameter to a compact set with no specified singularity. The system parameters were bounded by the maximum and minimum values to ensure that the singularity does not occur [19, 20]. In recent years, adaptive intelligent control algorithms have achieved high efficiency in controlling complex, time-varying, and highly nonlinear civil structures [21]. These algorithms mainly work on the principles of soft computing methods and artificial intelligence. The adaptive neural network (ANN) controller has recently achieved high efficiency in controlling the system with unknown dynamics [22]. Optimization associated with multiple control devices is considered a difficult task. Rashid et al. [23] proposed an adaptive algorithm based on acceleration response combined with a displacement optimization algorithm for 5-stage steel frames. However, the ANN controller often requires large amounts of computation. The unknown dynamics have been approximated by the radial basis function where the weights are optimal. However, this method cannot identify the parameters of the system such as mass, stiffness, and damping coefficient. Therefore, control strategies encompassing all the aforementioned controller's advantages and eliminating drawbacks should be designed to yield high-quality performance.

The major challenge with the semiactive device is the control force limitation and hysteresis state. The force constraint is a complicated problem because the maximum force value depends on the displacement and velocity value. Consequently, the actuator is inadequate in the controller requirements. Actuator limitations need special attention in the controller design. Recent studies have also mentioned this problem in engineering systems [24]. Hysteresis is a fundamental phenomenon in engineering. The semiactive vibration system usually exhibits a stable hysteretic state. The Bouc–Wen hysteresis model (BWM) is widely used to represent the properties of MR materials which have attracted researchers to develop intelligent vibration systems [25, 26]. The model is flexible and can be adjusted for different hysteretic states. BWM, with its flexibility in shape control, has been used to describe asymmetric hysteresis loops. The parametric modeling approach includes spring, damping, and Bouc–Wen models represented by a mathematical function. The coefficients of this function can be determined by using

an optimization technique. The parameter values are changed until the model's output force closely matches to the experimental output force. In contrast, nonparametric models are entirely based on the performance of a specific MR-based device, such as the neural network model and fuzzy model. These models are more flexible, but the physical relationship between modal parameters and hysteresis phenomena may not be explicitly maintained. These methods need large amounts of data and are performed in advance. We introduce a hysteresis observer to approximate the hysteresis state. The developed observer is expected to estimate the hysteresis quickly. The observer supports the controller to improve robustness against unmeasurable hysteresis. For practical applications, a novel controller is necessary to ensure the stability of a semiactive system.

In this study, we proposed an innovative control method to overcome the singularity in the traditional adaptive controller. The controller aims to exploit the advantages of adaptive controllers and neural network controllers and eliminate the disadvantages of these controllers with a smooth switching mechanism. Consequently, the denominator part of the adaptive control formula is absorbed near zero to eliminate the singularity problem. The adaptive controller is temporarily disabled in the event of a singularity occurring. An adaptive neural network controller is introduced to take over the system to ensure system stability. The displacement response converges to zero using the proposed controller, and the output control value can be remarkably reduced near the singularity condition. Firstly, a model was designed for the MRE-based isolator using the Bouc–Wen model, and an inverse model was developed to predict the desired current. Next, the ANN controller is used to estimate the uncertainty nonlinearity, and an adaptive controller (e.g., sliding adaptive controller) is designed to override the approximation error. A smooth switching algorithm is introduced to observe the singularity and determine the control authority between the ANN controller and a conventional adaptive controller. The new strategy is expected to avoid singularities, small control force, and fast stability. The novel adaptive controller includes five components:

(i) A robust adaptive controller is designed to ensure system stability.

(ii) An ANN controller is designed as the temporary controller in the singularity.

(iii) A smooth switching is used to exchange the takeover rights of the two controllers.

(iv) An auxiliary controller is developed to overcome the input constraint.

(v) Adaptive laws provide online estimates of the uncertain parameters without bounds, and a hysteresis observer is proposed to support the controller.

2. Magnetorheological Elastomer (MRE)

2.1. Model of MRE-Based Absorber. Three main materials used to fabricate the MRE samples included the matrix silicon RTV (68%) of the brand Shin-Etsu, carbon iron

powder with $20 \mu m$ diameter (30%) of the brand BASF SG-BH, and silicone oil (2%). MRE samples' fabrication procedures like natural rubber synthesis consist of mixing, compressing, molding, and curing. Firstly, these components were mixed to form a homogeneous mixture for 12 minutes. The mixture was placed in a vacuum chamber to remove air bubbles inside the material for 30 minutes. Finally, the mixture was vulcanized in a mold under a magnetic field or without a magnetic field for 24 hours at room temperature (26 degrees Celsius). Anisotropic MRE samples were vulcanized in a magnetic field, while isotropic MRE samples were vulcanized without a magnetic field. We use $25 \times 25 \times 8$ mm cube samples of MRE materials for the experiment.

The MRE-based absorber is used in this study, whose properties depend on displacement, amplitude, frequency, and magnetic field. In particular, its stiffness increases significantly when the applied current is increased. Consequently, the absorber operates efficiently over a wide range of frequencies presented in the research.

An MRE model is necessary for vibration system design; the hysteresis force-displacement loop is a major challenge under different applied currents. In this study, the Bouc–Wen model was used to present the behavior of MRE as shown in Figure 1. The model consists of a Bouc–Wen component and a Maxwell component. In the Bouc–Wen model, the evolutionary variable z describes the hysteresis behavior. The force of the MRE-based absorber is given by

$$F_{MRE} = \alpha k_0 x + c_0 \dot{x} + (1 - \alpha)k_0 z, \tag{1}$$

$$\dot{z} = A\dot{x} - \beta|\dot{x}||z|^{n-1}z - \gamma\dot{x}|z|^n, \tag{2}$$

where the linear stiffness force and purely hysteretic force are $\alpha k_0 x$ and $(1 - \alpha)k_0 z$, respectively. The coefficient, $\alpha \in (0, 1)$, represents the linearity level of the loop. The size and the shape of the hysteresis loops are determined by nondimensional parameters A, n, β, and γ as shown in equation (2). The parameter A has a significant influence on the force amplitude of the hysteresis, β and γ represent the shape of the hysteresis, and n is the order transition from linear to nonlinear state that was set to be one to reduce the amount of computation.

The variables of the model are approximated under the input current as follows [27, 28]:

$$k_0 = k_{0a} + k_{0b}I, \tag{3a}$$

$$c_0 = c_{0a} + c_{0b}I, \tag{3b}$$

$$\alpha = \alpha_a + a_bI, \tag{3c}$$

$$A = A_a + A_bI, \tag{3d}$$

$$\beta = \beta_a + \beta_bI, \tag{3e}$$

$$\gamma = \gamma_a + \gamma_bI. \tag{3f}$$

The model parameters were identified using a numerical optimization algorithm presented in Figure 2. The genetic algorithm is used to optimize the parameters of the Bouc–Wen model. The parameters were adjusted to fit the experimental data. Data were collected in many different cases (different frequency values, different current values, and different amplitude values). The fit values are listed in Table 1.

The MRE model, equation (1), is analyzed into three components: the viscous passive component, the active component F_a, and nonlinear hysteresis component Φ:

$$F_{MRE} = \alpha_a k_{0a} x + c_{oa}\dot{x} + \left((\alpha_a k_{0b} + \alpha_b k_{0a})I + \alpha_b k_{0b}I^2\right)x + c_{0b}I\dot{x} + (1 - \alpha)k_0 z$$
$$= \alpha_a k_{0a} x + c_{oa}\dot{x} + F_a + \Phi, \tag{4}$$

where

$$F_a = \left((\alpha_a k_{0b} + \alpha_b k_{0a})I + \alpha_b k_{0b}I^2\right)x + c_{0b}I\dot{x}, \tag{5a}$$

$$\Phi = (1 - \alpha)k_0 z. \tag{5b}$$

2.2. Experimental Tests and Validation. An experimental schematic was set up, as shown in Figure 3. The shear displacements were conducted with the sinusoidal function where the amplitudes were set from 0.4 mm to 0.8 mm and the frequencies were adjustable from 1 Hz to 20 Hz. The experiment was performed with various values of amperages from 0 A to 4 A. The displacement-force responses are compared between the measurement data and the numerical model with different current inputs and at the low-frequency case (1 Hz), as shown in Figure 4(a). In this case, the viscosity is very low, while the effect of hysteresis is very apparent. It can be seen that the effect of hysteresis is significant even at very low frequencies. The Bouc–Wen model with the appropriate parameters portrays very well the nonlinear hysteresis behavior. The viscous behavior was shown when performed at 10 Hz in Figure 4(b). The hysteresis loops tend to become elliptic as the applied current increases. Numerical responses and experimental results achieved a good agreement. The numerical model still achieves high accuracy when applying different current levels compared to the experiments, as shown in Figure 5. Based on the measured data, the current-dependent Bouc–Wen hysteretic model has fit the MRE isolator's dynamic behavior. Because the thickness of the MRE sample is small (0.8 mm), the value of the performance amplitude is also small. We perform at medium and large amplitudes according to 0.4 mm (5% shear stress) and 0.8 mm (10% shear stress), respectively. The
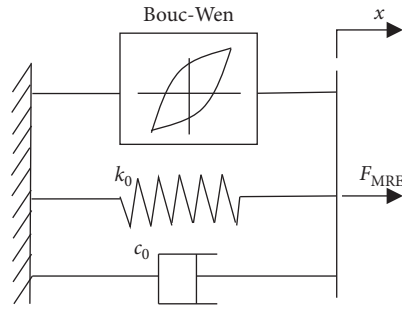
Figure 1: Schematic diagram of MRE-based isolator model.
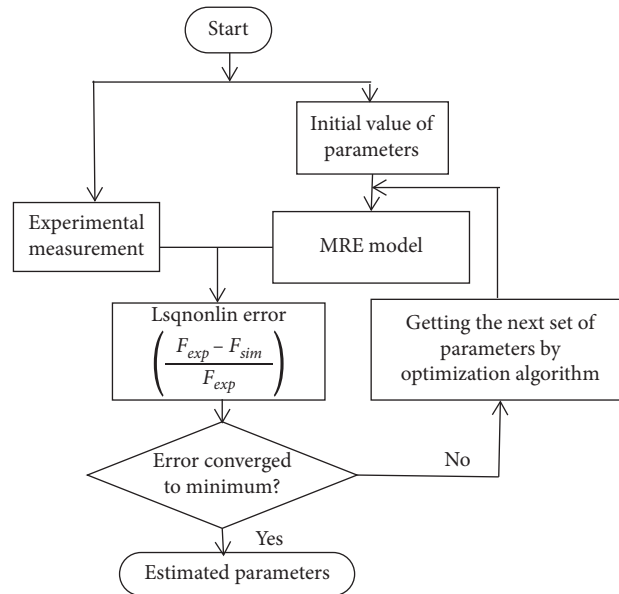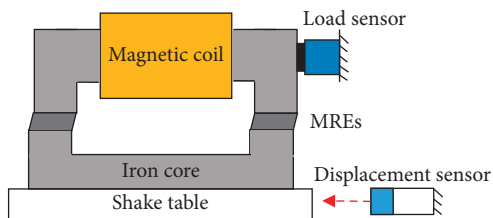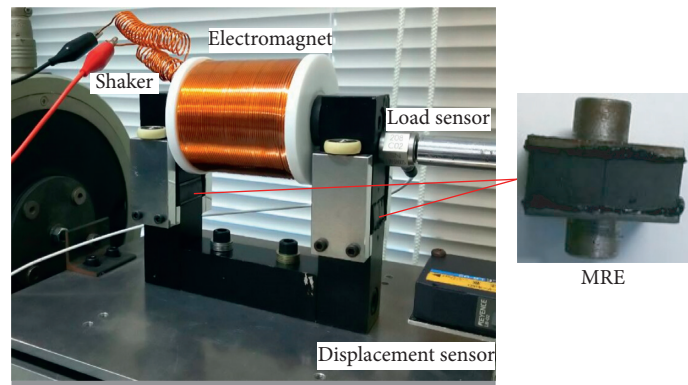

Figure 2: Flowchart of parameter identification using numerical optimization algorithm.

Table 1: Parameter values of MRE-based absorber using the Bouc–Wen model.

k_{0a}	c_{0a}	α_a	A_a	β_a	γ_a	k_{0b}	c_{0b}	a_b	A_a	β_a	γ_a
22	0.05	0.65	2	3.8	−1	12	0.01	0.05	0.2	0.33	0.3

(a)

(b)

Figure 3: Experimental schematic for collecting force-displacement data under different current values: (a) schematic; (b) photo.
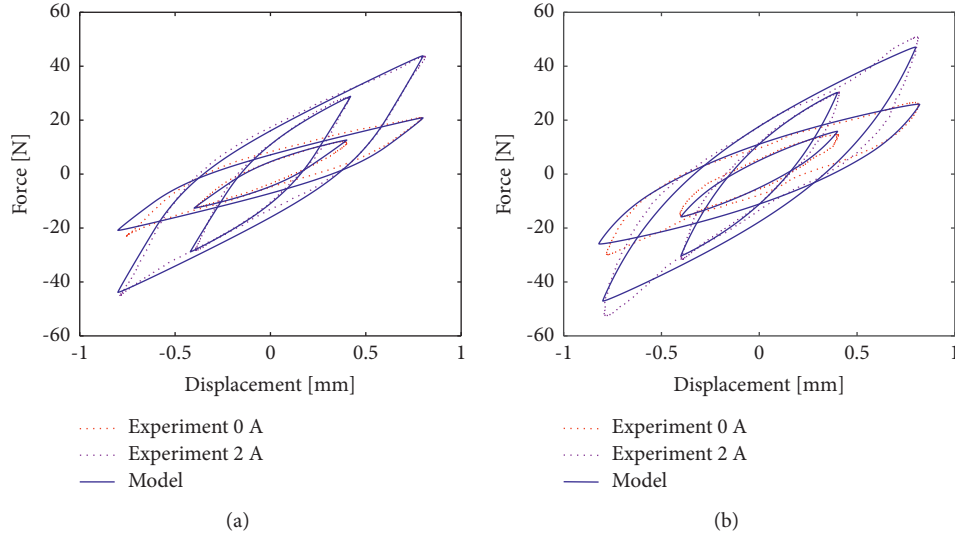
FIGURE 4: Force-displacement response under two displacement amplitude values ($x_0 = 0.4$ and 0.8) and two levels of applied current ($I = 0$ A (0 mT) and $I = 2$ A (218 mT)): (a) $f = 1$ Hz and (b) $f = 15$ Hz.
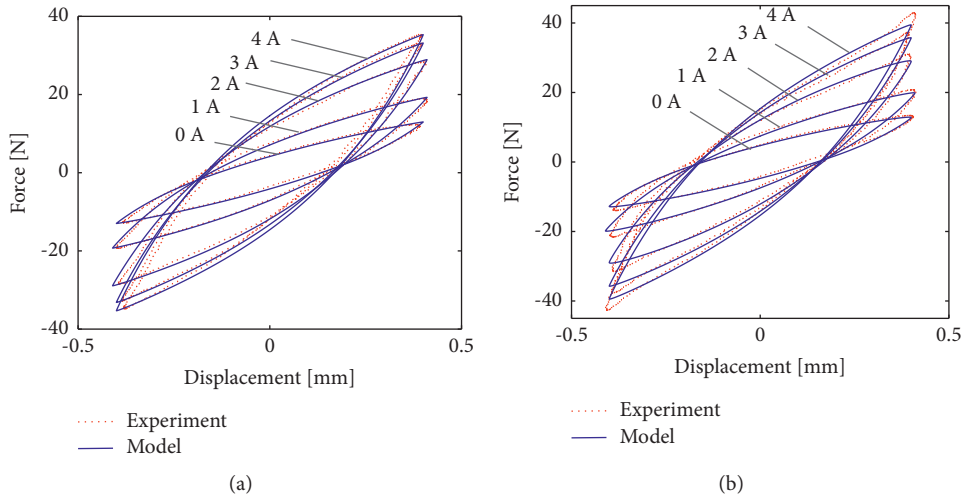

FIGURE 5: Force-displacement response under various applied currents ($I = 0$ A (0 mT), 1 A (109 mT), 2 A (218 mT), 3 A (325 mT), and 4 A (437 mT)): (a) $f = 1$ Hz and (b) $f = 15$ Hz.

isolator can perform up to 14% shear stress [14]. In the case of large amplitude performance, the MRE material sample thickness needs to be larger, and the magnetic system also needs to be enhanced to increase the system's efficiency.

2.3. Inversed Model. In practical applications, the inversed model is used to determine the input current/voltage for the isolator from the control force [17, 18, 29]. From equation (5a) and Table 1, the active force can be rewritten by variable amperage:

$$F_a = (\alpha_a k_{0b} + \alpha_b k_{0a} + c_{0b}\dot{x})I + (\alpha_b k_{0b}x)I^2$$
$$= (8.9 + 0.01\dot{x})I + (0.6x)I^2. \tag{6}$$

It is expected that the active force generated coincides with the control force, $F_a(t) = u(t)$. The input current is solved with the following equation and the electric current must be positive and $I \in [0, 4]$ ampere:

$$I^2(t) + \left(\frac{8.9 + 0.01\dot{x}(t)}{0.6x(t)}\right)I(t) - \frac{u(t)}{0.6x(t)} = 0, \tag{7}$$

where $u(t)$ is the control force determined by the proposed controller, $x(t)$ is measured by a displacement sensor, and velocity, $\dot{x}(t)$, is the first derivative of the displacement with respect to time.

The experiment was conducted under harmonic excitation. The applied current was adjusted to different values within the range of 0–4 A. The displacement data and force data were inputs of the MRE inverse model, as shown in Figures 6(a) and 6(b). The response current of the inverse model was compared with the measured current to evaluate the effectiveness of the model, as shown in Figure 6(c). The figure shows that the inverse model performed well in determining the current. The results demonstrate that the developed inverse model can convert the required control force into the value of current, which was fed to the MRE-based isolator.

3. Nonlinear Adaptive Control Design for Suspension Systems

3.1. A Quarter-Car Model Using MRE-Based Absorber. We consider the quarter-car model with MR elastomer as shown in Figure 7, and the system can be given by the following description.

The dynamic equations of the suspension system can be expressed as

$$m_s \ddot{x}_s + c_s (\dot{x}_s - \dot{x}_u) + k_s (x_s - x_u) + F_{MRE} = 0, \tag{8a}$$

$$\begin{aligned} m_u x_u + c_s (\dot{x}_u - \dot{x}_r) + k_s (x_u - x_s) \\ + k_u (x_u - x_r) - F_{MRE} = 0. \end{aligned} \tag{8b}$$

The absorber force, F_{MRE}, is modeled by equation (4) by using the Bouc–Wen model to describe the effect of the hysteresis, $\Phi = (1 - \alpha)k_0 z$, $A_\Phi = (1 - \alpha)k_0 A$. Let $u = F_a$ be a control input, and the sprung mass dynamics system equation (8a) can be rewritten as

$$\begin{aligned} m_s x_s + (c_s + c_{0a})(\dot{x}_s - \dot{x}_u) \\ + (k_s + \alpha_a k_{0a})(x_s - x_u) + u + \Phi = 0, \end{aligned} \tag{9a}$$

$$\dot{\Phi} = A_\Phi \dot{x} - \beta |\dot{x}| \Phi - \gamma \dot{x} |\Phi|^1. \tag{9b}$$

Assumption 1. The system parameters m_s, k_s, and c_s are uncertain and unbound. The component Φ represents the unmeasurable hysteresis. The control input is bounded by $[u_{\min}, u_{\max}]$.

Lemma 1 (see [30]). *For any $\epsilon > 0$ and $\eta \in R$, the inequality is introduced as*

$$0 \le |\eta| - \eta \tanh\left(\frac{\eta}{\epsilon}\right) \le \kappa \epsilon, \tag{10}$$

where $\kappa = 0.2785$ is the constant. To increase the smoothness of the system, the function $\mathrm{sat}(.)$ is replaced by $\tanh(.)$ in the robust controller.

3.2. Problem Statement. For the semiactive suspension system, many problems need to be dealt with in the controller design, and in this study, we consider the following aspects.

(1) *Ride Comfort.* In semiactive suspension design, stabilizing the vertical displacement is the main task in the controller's design which absorbs the maximum force of passengers.

(2) *Uncertain Parameters.* The system parameters such as mass, stiffness, and damping coefficient are uncertain and unbound. Singularity may occur during parameter adaptation, which can cause enormous forces or a faulty controller. A new adaptive controller needs to be designed to overcome the issue.

(3) *Actuator Saturation.* The control force is just active in the first and third of the force-displacement quadrant using an MRE-based absorber. The value of the force is also constrained by the maximum value and the minimum value.

(4) *Hysteresis State.* Hysteresis is a major problem in the MR system. This is a nonmeasurable component that greatly affects the stability of the system.

3.3. Adaptive Control Design

(a) The sliding control is defined as

$$S = \dot{x}_s + \lambda x_s, \tag{11}$$

where $\lambda > 0$ is the gain constant.

The time derivative of the sliding function S is as follows:

$$\dot{S} = \ddot{x}_s + \lambda \dot{x}_s. \tag{12}$$

Dynamic system equation (9) is written in terms of S:

$$\dot{S} = -b_1 u - b_1 \Phi - b_2 x_r - b_3 \dot{x}_r + \lambda x_s, \tag{13}$$

where $b_1 = 1/m_s$ $b_2 = 1/m_s(k_s + \alpha_a k_{0a})$; $b_3 = 1/m_s(c_s + c_{0a})$, $x_r = x_s - x_u$; and $\dot{x}_r = \dot{x}_s - \dot{x}_u$. Considering the fact that the system parameters b_1, b_2, b_3, and m_s are unknown in advance, the hysteresis state Φ is an unmeasurable component. To solve this problem, the parameters are estimated using the controller. The adaptive control force is proposed as

$$u = \frac{1}{\hat{b}_1}\left(kS - \hat{b}_2 x_r - \hat{b}_3 \dot{x}_r + \lambda x_s\right) - \hat{\Phi}, \tag{14}$$
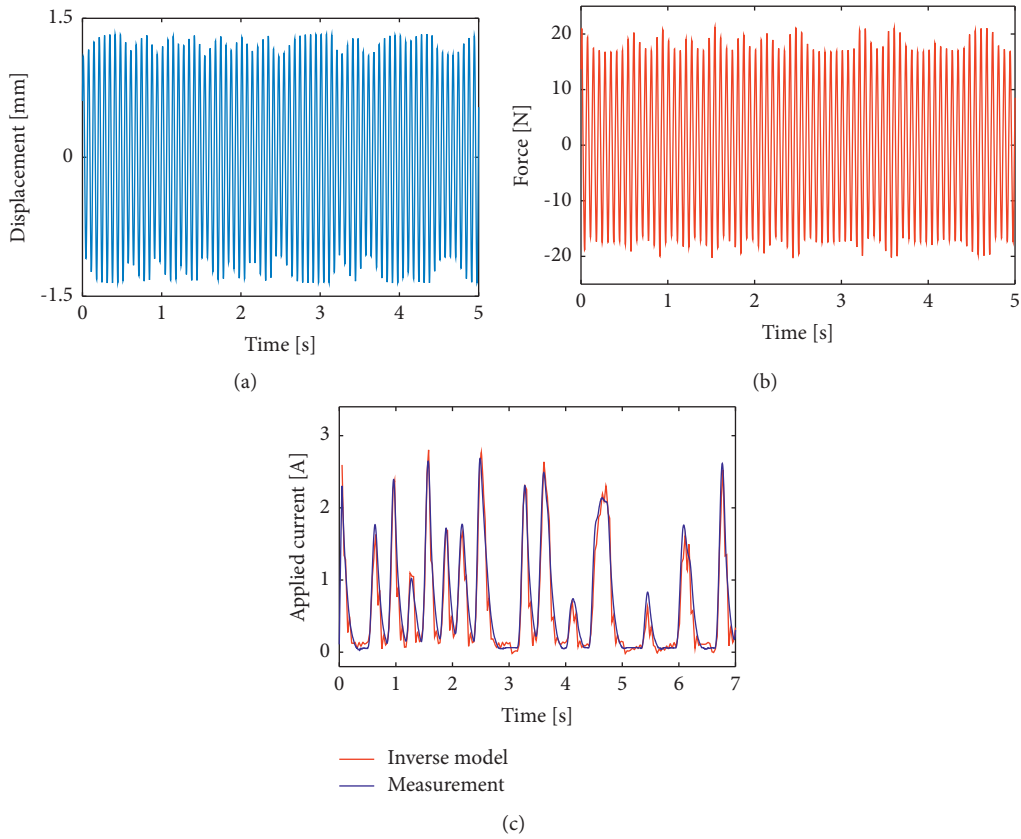
Figure 6: Applied current response using MRE inverse model: (a) displacement data, (b) force data, and (c) applied current response.
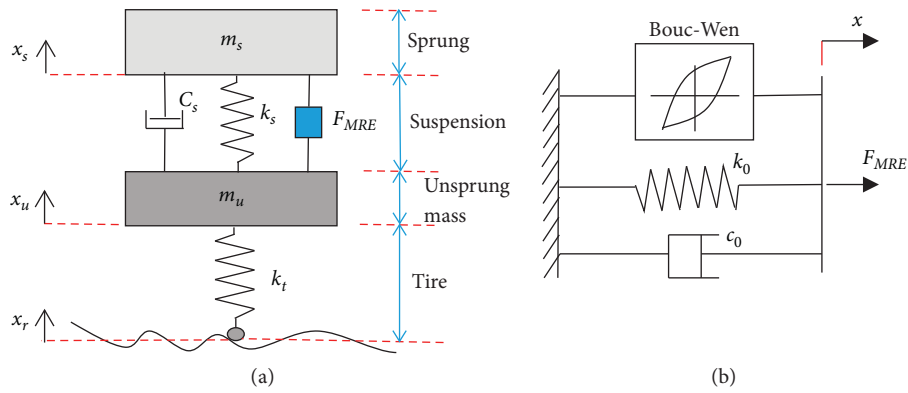

Figure 7: The novel suspension system using MRE-based absorber: (a) the suspension system and (b) the isolator model.

where $\widehat{b}_1$, $\widehat{b}_2$, and $\widehat{b}_3$ are the estimated values of the unknown model parameters b_1, b_2, and b_3, respectively, and k is a positive constant.

The controller is a significant dynamic variation in the plant. When the estimates parameter $\widehat{b}_1$ reach around zero or $\widehat{b}_2$, $\widehat{b}_3$ achieve large values, the control force becomes a large value; if $\widehat{b}_1 \longrightarrow 0$ or $\widehat{b}_2 \longrightarrow \infty$ or $\widehat{b}_3 \longrightarrow \infty$, then $u \longrightarrow \infty$. This problem will greatly affect the stability of the system [31].

(b) Adaptive neural network control.

We applied the radial basis function (RBF) neural network $W^T Z(S)$ that can estimate the function $f(S) = b_1^{-1}(-b_2 x_r - b_3 \dot{x}_r + \lambda x_s)$ with arbitrary accuracy, such that

$$b_1^{-1}\left(-b_2 x_r - b_3 \dot{x}_r + \lambda x_s\right) = W_c^T Z(S) + \varepsilon_c, \quad \forall x \in D, \tag{15}$$

where $W_c = [w_1, w_2, \ldots, w_N]^T$ is an optimal constant weight vector, $N > 1$ is the number of the neurons, $Z(S) = [z_1(S), z_2(S), \ldots, x_N(S)]^T$ is the RBF vector, and ε_c is error that is optimized by the vector W.

The weight vector W is updated to minimize ε_c on the compact set D:

$$W := \underset{W \in R}{\operatorname{argmin}} \left\{ \underset{x \in D}{\sup} \left| f(S) - W_c^T Z(S) \right| \right\}. \tag{16}$$

Assume that ε_c is bounded by $|\varepsilon_c| < \varepsilon^*$ with ε^* being an unknown positive constant. The Gaussian function, $z_i(x)$, is given by

$$z_i(S) = \exp\left[\frac{-(S - \gamma_i)^T (S - \gamma_i)}{\omega_i^2} \right], \tag{17}$$

where γ_i and ω_i represent the center and width of the function, respectively.

The adaptive neural network controller was designed, u_{ann}, for the nonlinear uncertain part of the suspension system:

$$u_{ann} = \widehat{W}_c^T Z(S) + \widehat{\varepsilon}_c + kS. \tag{18}$$

The controller has a capacity in predicting model nonsingularities on a compact set D and achieving a good performance in nonlinear identification. However, the controller takes up a lot of computation and takes a long time to process. The system parameters, such as stiffness, mass, and damping coefficient, cannot be identified by using this method.

3.4. Smooth Switching Adaptive Controller.
A control strategy that encompasses all advantages of the controller mentioned above and eliminates the drawbacks is proposed in this study. The block diagram of the controller is shown in

Figure 8. First, the smooth switching algorithm is introduced in this study to observe the singularity and to determine the authority of the two above controllers:

$$\eta(b) = 1 - \exp\left(-\left(\frac{b}{\delta}\right)^2 \right), b$$

$$= \min\left\{ |\widehat{b}_1|, \frac{1}{|\widehat{b}_2|}, \frac{1}{|\widehat{b}_3|} \right\}, \forall \widehat{b}_1, \widehat{b}_2, \widehat{b}_3 \in R, \tag{19}$$

where b is the variable that causes the singularity and δ is the width of the corresponding transition. The switching algorithm has the following characteristics:

$$\text{C1.} \, 0 \le \eta(b) \le 1 \, \forall \widehat{b}_1 \in R, \tag{20a}$$

$$\text{C2.} \, \lim_{b \longrightarrow 0} \eta(b) = 0, \tag{20b}$$

$$\text{C3.} \, \lim_{b \longrightarrow 0} \eta(b) = 1, \tag{20c}$$

$$\text{C4.} \, \lim_{\widehat{b}_1 \longrightarrow 0} \frac{\eta(b)}{\widehat{b}_1} = 0, \, \lim_{\widehat{b}_2 \longrightarrow \infty} \left[\eta(b) \times \widehat{b}_2 \right]$$
$$= 0, \, \lim_{\widehat{b}_3 \longrightarrow \infty} \left[\eta(b) \times \widehat{b}_3 \right] = 0. \tag{20d}$$

Furthermore, to support the controller, an observer was developed to estimate the hysteresis state Φ that can be described by

$$\dot{\widehat{\Phi}} = A_{\Phi} \dot{x} - \beta |\dot{x}| \widehat{\Phi} - \gamma \dot{x} |\widehat{\Phi}| + \vartheta, \tag{21}$$

where ϑ is the observer dynamic component suggested later. Suppose the observation error is defined as $\widetilde{\Phi} = \widehat{\Phi} - \Phi$, and the observation misalignment is determined as follows:

$$\dot{\widetilde{\Phi}} = \dot{\widehat{\Phi}} - \dot{\Phi} = -\beta |x| \widetilde{\Phi} - \gamma \dot{x} \left(|\widehat{\Phi}| - |\Phi| \right) + \vartheta. \tag{22}$$

A switching adaptive control algorithm is proposed as follows:

$$u_c = \eta u_a + (1 - \eta) u_{ann} - \widehat{\Phi}, \tag{23}$$

where

$$u_a = \left(\widehat{b}_1\right)^{-1} \left(kS - \widehat{b}_2 x_r - \widehat{b}_3 \dot{x}_r + \lambda x_s \right), \tag{24}$$

$$u_{ann} = \widehat{W}_c^T Z(S) + \widehat{\varepsilon}_c + kS, \tag{25}$$

where $\widehat{b}_1$, $\widehat{b}_2$, and $\widehat{b}_3$ are estimated values of the unknown model parameters b_1, b_2, and b_3, respectively. The error responses were defined as $\widetilde{b}_1 = \widehat{b}_1 - b_1$, $\widetilde{b}_2 = \widehat{b}_2 - b_2$, and $\widetilde{b}_3 = \widehat{b}_3 - b_3$. The hysteresis observer $\widehat{\Phi}$ is developed for the proposed controller.

The force of MRE-based absorber is limited by the maximum and minimum values [32]. The input control force of the system is satisfied with the following requirements:
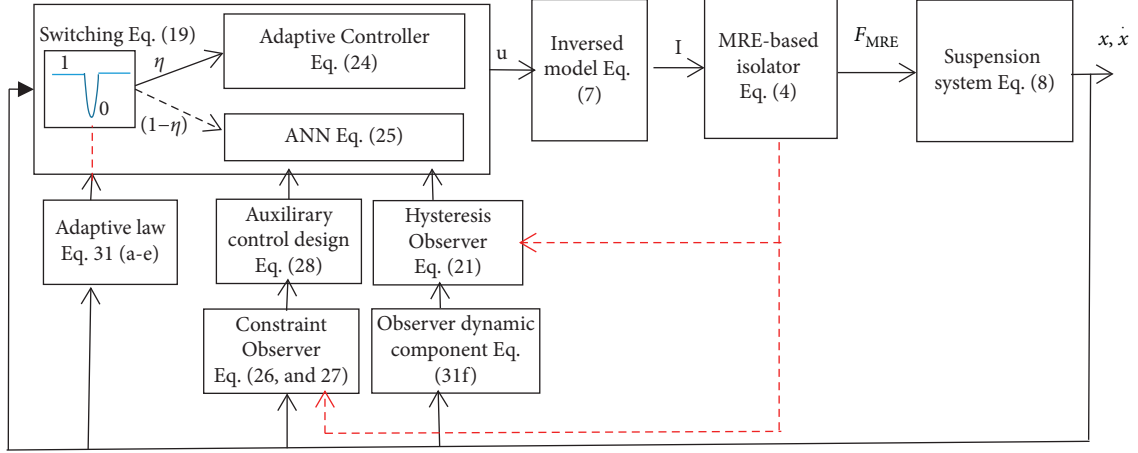
FIGURE 8: Block diagram of the proposed controller.

$$u = \begin{cases} u_{\max} & if \quad u_c > u_{\max} \\ u_{\min} & if \quad u_c < u_{\min} \\ u_c & if \quad u_{\max} < u_c < u_{\max} \end{cases}, \quad (26)$$

and

$$\delta = \begin{cases} u_c - u_{\max} & if \quad u_c > u_{\max} \\ u_c - u_{\min} & if \quad u_c < u_{\min} \\ 0 & if \quad u_{\max} < u_c < u_{\max} \end{cases}, \quad (27)$$

where $u_{\max}$ and $u_{\min}$ are determined by using equation (5a), $u_{\max} = F_a(I_{\max})$ if $F_a > 0$, $u_{\min} = F_a(I_{\max})$ if $F_a < 0$, the direction of F_a depends on x_r, δ is the amount of value that exceeds the limits of the controller, ξ is a regulator to ensure the system is stable, u is the actual force, and u_c is the desired control force. The absorber force fails to meet the control force due to actuator limitations in many cases. In this study, the following auxiliary design system is proposed to regulate the phenomenon:

$$\dot{\xi} = \begin{cases} -k_\lambda \xi - \dfrac{S\delta + |\xi|}{\xi} + \tanh\left(\dfrac{\xi}{\epsilon}\right) & |\xi| \geq \mu \\ \\ 0 & |\xi| \leq \mu \end{cases}, \quad (28)$$

where $\xi \in R$ is an auxiliary design system state, $K_\lambda \in R^+$, and μ is a small positive value.

The auxiliary controller u_{au} that satisfies the constraint of MRE isolator is added as

$$u_{au} = -\delta - \xi. \quad (29)$$

Finally, the controller proposed in this study consists of four components including the adaptive controller u_a, the adaptive neural network controller u_{ann}, the auxiliary controller u_{au}, and the smooth switching $\eta(b)$:

$$u = \eta u_a + (1 - \eta)u_{ann} + u_{au} - \widehat{\Phi}. \quad (30)$$

The updated laws for the parameters are proposed as follows:

$$\dot{\widehat{b}}_1 = c_1 \frac{\eta}{\widehat{b}_1} S\left(kS - \widehat{b}_2 x_r - \widehat{b}_3 \dot{x}_r + \lambda x_s\right), \quad (31a)$$

$$\dot{\widehat{b}}_2 = c_2 \eta S x_r, \quad (31b)$$

$$\dot{\widehat{b}}_3 = c_3 \eta S \dot{x}_r, \quad (31c)$$

$$\dot{\widehat{W}}_c = c_4(1 - \eta) S Z(S), \quad (31d)$$

$$\dot{\widehat{\varepsilon}}_c = c_5(1 - \eta)S. \quad (31e)$$

The dynamic component of the hysteresis state can be regulated as

$$\vartheta = -c_6 S. \quad (31f)$$

Remark 1. Regarding property characteristic C4, we see that the singularity is eliminated, which means $\widehat{b}_1 \longrightarrow 0$, $\widehat{b}_2 \longrightarrow \infty$, $\widehat{b}_3 \longrightarrow \infty$, $\lim\limits_{\widehat{b}_1 \to 0} \eta(b)/\widehat{b}_1 = 0$, $\lim\limits_{\widehat{b}_2 \to \infty}$ $[\eta(b) \times \widehat{b}_2] = 0$, and $\lim\limits_{\widehat{b}_3 \to \infty} [\eta(b) \times \widehat{b}_3] = 0$. As a result, adaptive control signal equation (24) and adaptive signal equation (31a) are bounded. Hence, the singularity is totally avoided. Furthermore, the smooth switching algorithm ensures continuous signals. The chattering is also reduced by switching.

4. Stability Analysis

Theorem 1. *Consider the vibration system ((8a) and (8b)) with the sliding function given by (9a) and (9b) under the novel adaptive controller (30) and the updated laws (31a)–(31e) such that all signals are bounded and the system is stable.*

Proof. Lyapunov function candidate is selected as

$$
V = \frac{1}{2}S^2 + \frac{1}{2c_1}\tilde{b}_1^2 + \frac{1}{2c_2}\tilde{b}_2^2 + \frac{1}{2c_3}\tilde{b}_3^2 + \frac{1}{2c_4}b_1\tilde{W}_c^2
$$
$$
+ \frac{1}{2c_5}b_1\tilde{\varepsilon}_c^2 + \frac{1}{2c_6}b_1\tilde{\Phi}^2 + \frac{1}{2}b_1\xi^2. \tag{32}
$$

With the time derivative of Lyapunov function and application of equation (30), we have

$$
\dot{V} = S\dot{S} + \frac{1}{c_1}\tilde{b}_1\dot{\tilde{b}}_1 + \frac{1}{c_2}\tilde{b}_2\dot{\tilde{b}}_2 + \frac{1}{c_3}\tilde{b}_3\dot{\tilde{b}}_3 + \frac{1}{c_4}b_1\tilde{W}_c\dot{\tilde{W}}_c + \frac{1}{c_5}b_1\tilde{\varepsilon}_c\dot{\tilde{\varepsilon}}_c + \frac{1}{c_6}b_1\tilde{\Phi}\dot{\tilde{\Phi}} + b_1\xi\dot{\xi}
$$

$$
= S[-b_1 u - b_1\Phi - b_2 x_r - b_3\dot{x}_r + \lambda x_s] + \frac{1}{c_1}\tilde{b}_1\dot{\tilde{b}}_1 + \frac{1}{c_2}\tilde{b}_2\dot{\tilde{b}}_2 + \frac{1}{c_3}\tilde{b}_3\dot{\tilde{b}}_3 + \frac{1}{c_4}b_1\tilde{W}_c\dot{\tilde{W}}_c + \frac{1}{c_5}b_1\tilde{\varepsilon}_c\dot{\tilde{\varepsilon}}_c + \frac{1}{c_6}b_1\tilde{\Phi}\dot{\tilde{\Phi}} + b_1\xi\dot{\xi}
$$

$$
= S[-b_1(\eta u_a + (1-\eta)u_{ann} + u_{au} - \widehat{\Phi}) - b_1\Phi - b_2 x_r - b_3\dot{x}_r + \lambda x_s] + \frac{1}{c_1}\tilde{b}_1\dot{\tilde{b}}_1 + \frac{1}{c_2}\tilde{b}_2\dot{\tilde{b}}_2 + \frac{1}{c_3}\tilde{b}_3\dot{\tilde{b}}_3 + \frac{1}{c_4}b_1\tilde{W}_c\dot{\tilde{W}}_c + \frac{1}{c_5}b_1\tilde{\varepsilon}_c\dot{\tilde{\varepsilon}}_c
$$

$$
+ \frac{1}{c_6}b_1\tilde{\Phi}\dot{\tilde{\Phi}} + b_1\xi\dot{\xi}, \tag{33}
$$

$$
\dot{V} = \dot{V}_1 + \dot{V}_2 + \dot{V}_3 + \dot{V}_4, \tag{34}
$$

where each term on right-hand side of the function is written explicitly as follows.

We apply the inequality $(|\Phi| - |\widehat{\Phi}|) \le |\widehat{\Phi} - \Phi| = |\tilde{\Phi}|$ and the observer dynamics component equation (31f), $\vartheta = -c_6 S$, to V_1:

$$
\dot{V}_1 = S b_1(\widehat{\Phi} - \Phi) + \frac{1}{c_6}b_1\tilde{\Phi}\dot{\tilde{\Phi}}
$$

$$
= b_1\left(S\tilde{\Phi} + \frac{1}{c_6}\tilde{\Phi}(-\beta|x|\tilde{\Phi} - \gamma x(|\widehat{\Phi}| - |\Phi|)) + \vartheta\right)
$$

$$
\le b_1\left(S\tilde{\Phi} - \frac{1}{c_6}\beta|x|\tilde{\Phi}^2 + \frac{1}{c_6}\gamma|x|\tilde{\Phi}^2 + \frac{1}{c_6}\tilde{\Phi}\vartheta\right) \tag{35}
$$

$$
= -\frac{b_1}{c_6}(\beta - \gamma)|x|\tilde{\Phi}^2,
$$

where $b_1 > 0$, $\gamma > 0$, $\beta - \gamma > 0$ in Table 1.

Next, adaptive algorithm equations (31a)–31c are applied to $\dot{V}_2$:

$$
\begin{aligned}
\dot{V}_2 &= \eta S\left(-b_1 u_a - b_2 x_r - b_3 \dot{x}_r + \lambda x_s\right) + \frac{1}{c_1}\tilde{b}_1 \dot{\hat{b}}_1 + \frac{1}{c_2}\tilde{b}_2 \dot{\hat{b}}_2 + \frac{1}{c_3}\tilde{b}_3 \dot{\hat{b}}_3 \\
&= \eta S\left(-\left(\hat{b}_1 - \tilde{b}_1\right)\frac{1}{\hat{b}_1}\left(kS - \hat{b}_2 x_r - \hat{b}_3 \dot{x}_r + \lambda x_s\right) - b_2 x_r - b_3 \dot{x}_r + \lambda x_s\right) + \frac{1}{c_1}\tilde{b}_1 \dot{\hat{b}}_1 + \frac{1}{c_2}\tilde{b}_2 \dot{\hat{b}}_2 + \frac{1}{c_3}\tilde{b}_3 \dot{\hat{b}}_3 \\
&= -\eta k S^2 - \eta S x_r\left(\hat{b}_2 - b_2\right) - \eta S \dot{x}_r\left(\hat{b}_3 - b_3\right) - \eta S \frac{\tilde{b}_1}{\hat{b}_1}\left(k_s S - \hat{b}_2 x_r - \hat{b}_3 \dot{x}_r + \lambda x_s\right) + \frac{1}{c_1}\tilde{b}_1 \dot{\hat{b}}_1 + \frac{1}{c_2}\tilde{b}_2 \dot{\hat{b}}_2 + \frac{1}{c_3}\tilde{b}_3 \dot{\hat{b}}_3 \quad (36) \\
&= -\eta k S^2 - \tilde{b}_2\left(\eta S x_r - \frac{1}{c_2}\dot{\hat{b}}_2\right) - \tilde{b}_3\left(\eta S \dot{x}_r - \frac{1}{c_3}\dot{\hat{b}}_3\right) - \tilde{b}_1\left(\eta\left(\hat{b}_1\right)^{-1}S\left(k_s S - \hat{b}_2 x_r - \hat{b}_3 \dot{x}_r + \lambda x_s\right) + \frac{1}{c_1}\dot{\hat{b}}_1\right) \\
&= -\eta k S^2.
\end{aligned}
$$

Adaptive algorithm equations (31d)–31e are applied to $\dot{V}_3$:

$$
\begin{aligned}
\dot{V}_3 &= (1-\eta)S\left(-b_1 u_{ann} - b_2 x_r - b_3 \dot{x}_r + \lambda x_s\right) + \frac{1}{c_4}\tilde{W}_c \dot{\hat{W}}_c + \frac{1}{c_5}\tilde{\varepsilon}_c \dot{\hat{\varepsilon}}_c \\
&= (1-\eta)S\left(-b_1\left(\hat{W}_c^T Z(z) + \hat{\varepsilon}_c + kS\right) - b_1\left(W_c^T Z(z) + \varepsilon_c\right)\right) + \frac{1}{c_4}b_1 \tilde{W}_c \dot{\hat{W}}_c + \frac{1}{c_5}b_1 \tilde{\varepsilon}_c \dot{\hat{\varepsilon}}_c \\
&= -(1-\eta)b_1 kS^2 + b_1\left[(1-\eta)S\left(-\hat{W}_c^T Z(z) + \left(W_c^T Z(z)\right)\right)\right] + b_1\left[(1-\eta)S\left(-\hat{\varepsilon}_c + \varepsilon_c\right)\right] + \frac{1}{c_4}b_1 \tilde{W}_c \dot{\hat{W}}_c + \frac{1}{c_5}b_1 \tilde{\varepsilon}_c \dot{\hat{\varepsilon}}_c \quad (37) \\
&= -(1-\eta)b_1 kS^2 + b_1 \tilde{W}_c\left[-(1-\eta)S Z(z) + \frac{1}{c_4}\dot{\hat{W}}_c\right] + b_1 \tilde{\varepsilon}_c\left[-(1-\eta)S + \frac{1}{c_5}\dot{\hat{\varepsilon}}_c\right] \\
&= -(1-\eta)b_1 kS^2.
\end{aligned}
$$

The auxiliary design system equation (29) and Lemma 1 are applied to $\dot{V}_4$:

$$
\begin{aligned}
\dot{V}_4 &= -b_1 S u_{au} + \xi \dot{\xi} \\
&= -b_1 S(-\delta - \xi) + b_1 \xi\left[-k_\lambda \xi - \frac{S\delta + |\xi|}{\xi} + \tanh\left(\frac{\xi}{\epsilon}\right)\right] \quad (38) \\
&= -b_1 k_\lambda \xi^2 - b_1\left[|\xi| - \xi \tanh\left(\frac{\xi}{\epsilon}\right)\right] \\
&= -b_1 k_\lambda \xi^2 - \kappa,
\end{aligned}
$$

where ϵ is a positive constant and $\kappa = 0.2785$, $|\xi| - \xi \tanh(\xi/\epsilon) \leq \kappa\epsilon$.

Applying equations (35)–(38), the derivative Lyapunov equation (34) is represented as

$$
\dot{V} < -\frac{b_1}{c_6}(\beta - \gamma)|x|\tilde{\Phi}^2 - \eta k S^2 - (1-\eta)b_1 kS^2 - b_1 k_\lambda \xi^2 - \kappa\epsilon < 0. \quad (39)
$$

The boundedness of $\tilde{b}_1$, $\tilde{b}_2$, $\tilde{b}_3$, $\tilde{\Phi}$, and S is asymptotic to zero by the Lyapunov stability criterion. Therefore, the closed-loop system is asymptotically stable. Associated with Remark 1, all signals are bounded.

5. Simulations

In this section, the system, combined with the proposed controller, is simulated to reduce the vibration effectiveness. The dynamic system's parameter values are assigned as $m_s = 2.45$ kg, $m_u = 1$ kg, $k_s = 900$ m^{-1}, $c_s = 8$ N s m^{-1}, $k_t = 2500$ N m^{-1}, and the parameters of MRE model are shown in Table 1; the initial state $[b_1, b_2, b_3] = [0.01, 0.01, 0.01]$, and $[x_s, \dot{x}_s, x_u, \dot{x}_u] = [0, 0, 0, 0]$. The coefficients of the
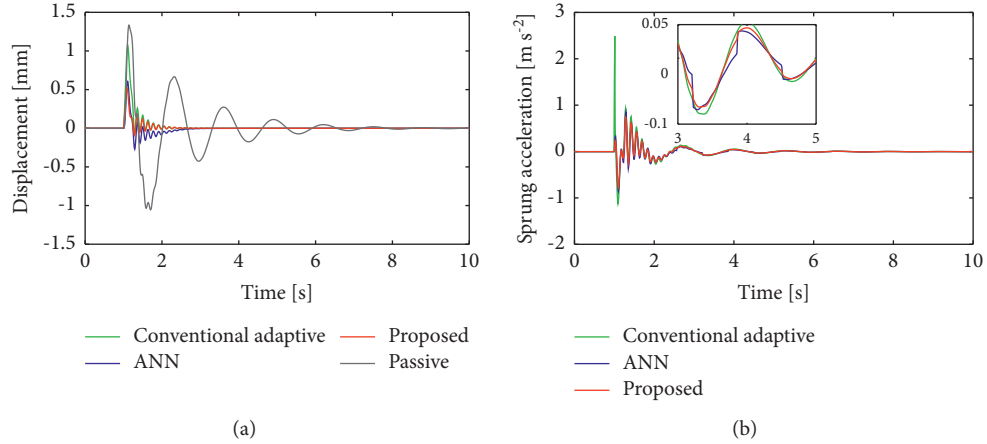
FIGURE 9: The comparison of sprung mass responses under bump wheel excitation for three different strategies: (a) displacement response and (b) acceleration response.

controller are selected as $c_1 = 2$; $c_2 = 2$; $c_3 = 2$; $c_4 = 4$; $c_5 = 4$; $c_6 = 1$; $\lambda = 2$; and $\delta = 0.1$. Four strategies have been investigated to evaluate controllers: conventional adaptive controller, adaptive neural network controller, the switching adaptive controller (proposed controller), and passive controller. We used the Runge–Kutta 4th order method to solve the differential equation.

5.1. Bump Wheel Excitation. The relative displacement and mass acceleration responses are depicted in Figure 9 for four cases including conventional adaptive controller, ANN controller, proposed controller, and passive system. The relative displacement is reduced significantly using the controllers. The efficiency is the same for the acceleration response, as shown in Figure 9(b). Furthermore, the response is smoother when it reaches a steady state by using the proposed controller.

The switching signal and control forces are shown in Figures 10 and 11, respectively. The switching signal indicates that the adaptive neural network controller takes over in about 1.5 seconds, and then the adaptive controller gradually dominates the controller. Figure 11 presents the control force of the three strategies. From the figure, the proposed controller required a small control effort than the single controller, while the control force jumped to a large value when $\hat{b}_1$ was near zero using the conventional adaptive controller.

The adaptive parameters and hysteresis state are shown in Figures 12 and 13. From the figures, the parameters achieve a stable state after 2 seconds. The input current calculated by using the proposed algorithm is shown in Figure 14. If the actual force achieves a maximum value, the applied current is set at four amperages. In other cases, the inverse model is used to calculate the required current. These results demonstrate that the proposed controller achieves high efficiency compared to conventional controllers to reduce system vibration.

5.2. Random Road Displacement. To further validate the proposed strategy under random excitation, we choose the road disturbance with an amplitude of 5 mm. From Figure 15, we found that the controllers work well, and the mass displacement responses approach zero quickly. The proposed controller has achieved a positive result while avoiding the drawbacks of the traditional adaptive controllers. The control force, smooth switching, hysteresis state, and applied current are also shown in Figures 16–19. The force generated by the MRE-based isolator is compared for different strategies in Figure 16, where the proposed controller needs a smaller value compared to the other controllers. At the initial time, the hysteresis value is unknown, and the measurement is not achievable. Using an adaptive observer, the value of the hysteresis is estimated and updated based on the hysteresis dynamics equation (31f). Results are depicted in Figure 19 after 0.2 seconds to verify the hysteresis state estimation. The observer has portrayed well the hysteresis properties by using the hysteresis state dynamics.

The efficiency of the proposed controller is based on its adaptability. In the early stages of the control process, the adaptive parameters are in a highly dynamic state, so a singularity phenomenon may occur in this state. The system is dominated temporarily by the ANN controller so that the system works stably and safely. In this stage, the traditional adaptive controller still works as the virtual controller, and the parameters are continuously adapted. When the adaptive values are out of the singularity, the adaptive controller smoothly takes over the system, and the adaptive values update to their true values quickly. A smooth switching algorithm is used to observe the adaptive parameters and decide which controller takes over the system. The smooth switching algorithm has outstanding advantages. When the signals pass through the singularity, the algorithm can suppress this phenomenon, and the controller is temporarily switched to the ANN controller. In this way, the advantages of a single controller are exploited, and their disadvantages are eliminated.
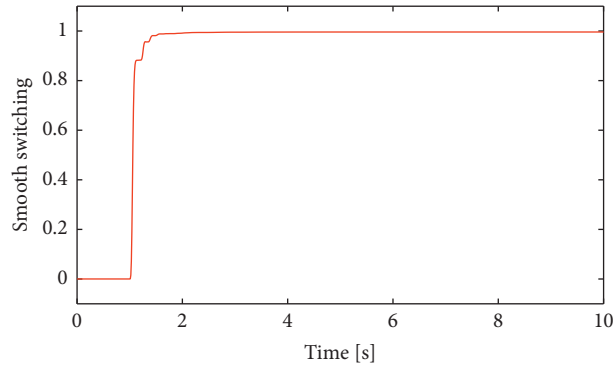
FIGURE 10: The smooth switching to take over between the controllers under bump wheel excitation.
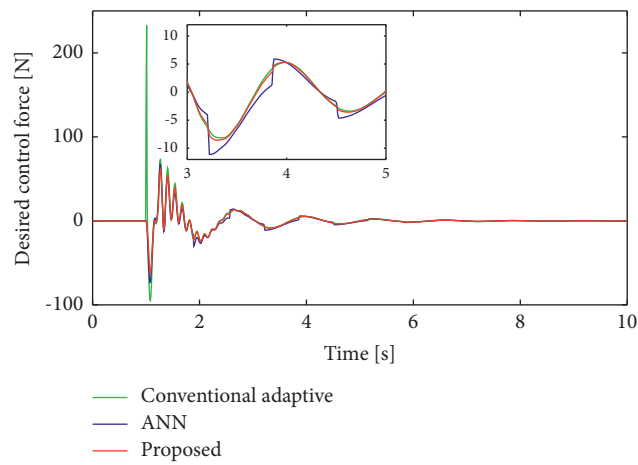

FIGURE 11: The comparison of control force for the system with the proposed algorithm.
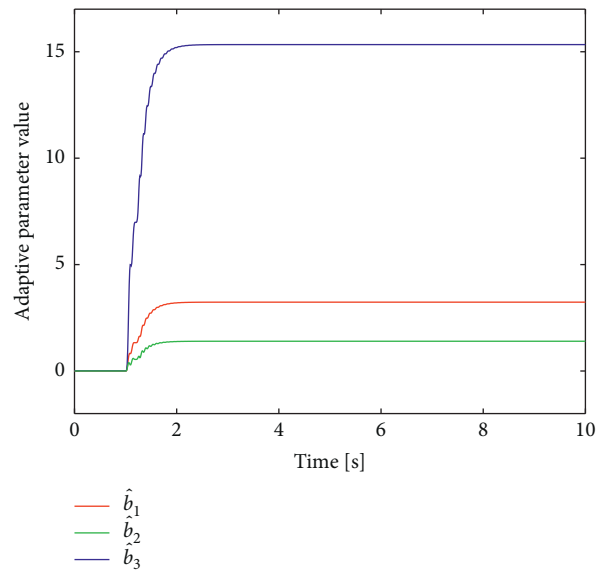

FIGURE 12: Time history of the adaptive parameters $\hat{b}_1$, $\hat{b}_2$, and $\hat{b}_3$.
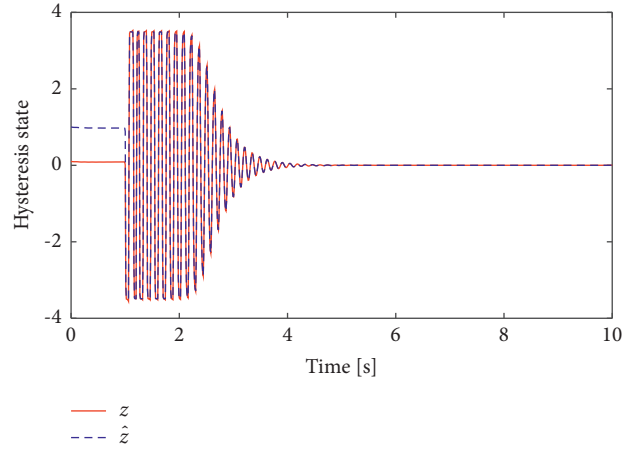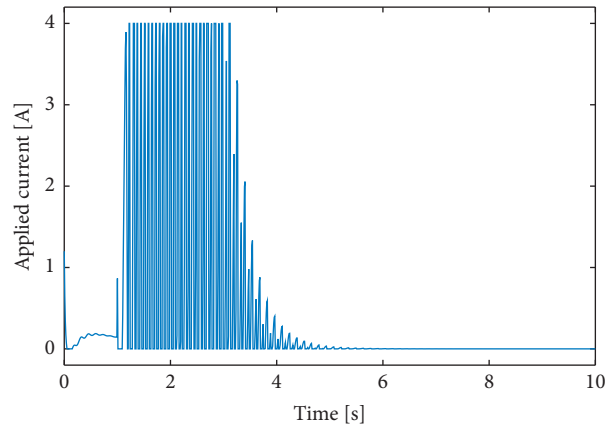
Figure 13: Time history of the hysteresis state.

Figure 14: Current input for the system with the proposed algorithm.
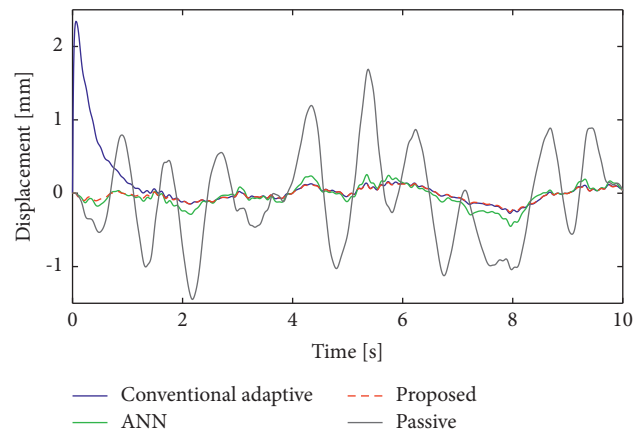

Figure 15: The comparison of sprung mass displacement responses under random excitation for three different strategies.
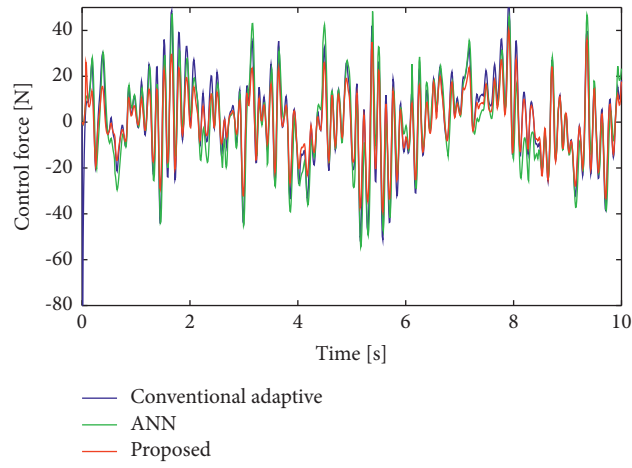
Figure 16: The comparison of control forces for the system for three different strategies.
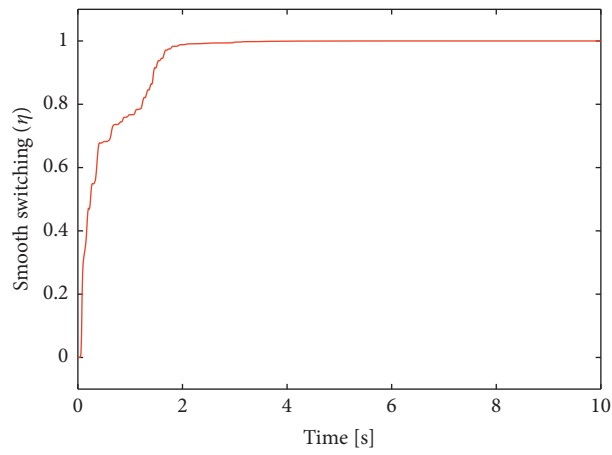

Figure 17: The smooth switching to take over between the controllers under random excitation.
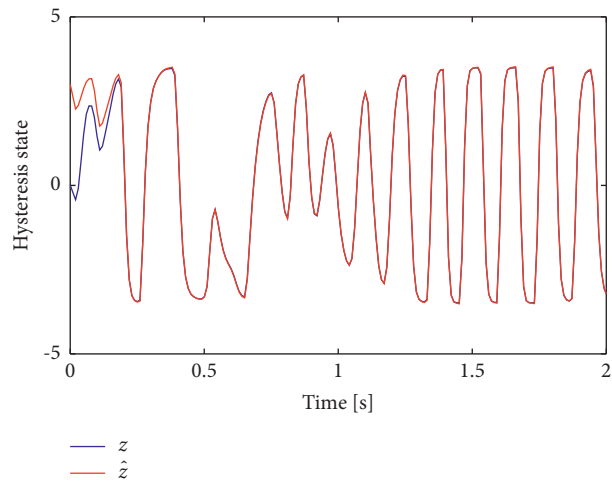

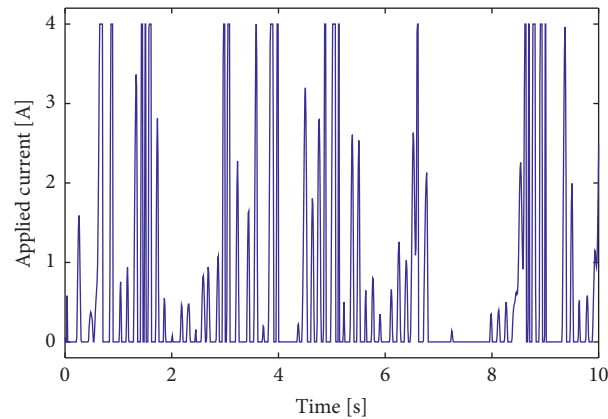Figure 18: Time history of the hysteresis state.

FIGURE 19: Current input for the system with the proposed algorithm.

6. Conclusions

In this study, the Bouc–Wen model was used to represent the properties of the MRE material. The inverse model was also developed to determine the applied current for the MRE-based isolator. A nonlinear observer was constructed to predict the unknown hysteresis state, and the input constraint was also considered to ensure the system's stability. The control singularity was avoided with such an approach, and the transient behavior improved in the adaptive controller. Based on the unique characteristics of smooth switching equations (20a)–20d, the controller requires less force without loss performance than the single controller. The proposed controller exploited the advantages of adaptive controllers and neural network controllers and eliminated the disadvantages of these controllers with a smooth switching mechanism. Consequently, the denominator part of the adaptive control formula was absorbed near zero to eliminate the singularity problem. The proposed controller overcomes the traditional adaptive controller's disadvantages, including nonsingularity, low control force, and high stability. The simulation results have proved the effectiveness of the proposed control algorithm. The proposed controller significantly improves the vibration system compared to the adaptive controller.

Data Availability

The data used to support the findings of this study are available upon request from the corresponding author.

Conflicts of Interest

The authors declare that they have no conflicts of interest.

References

[1] Y. Li, J. Li, W. Li, and H. Du, "A state-of-the-art review on magnetorheological elastomer device," *Smart Materials and Structures*, vol. 23, no. 12, pp. 1–24, 2014.

[2] J. M. Ginder, M. E. Nichols, L. D. Elie, and J. L. Tardiff, "Magnetorheological elastomers: properties and applications," in *Proceedings of the SPIE 3675, Smart Structures and Materials 1999: Smart Materials Technologies*, pp. 131–138, Newport Beach, USA, July 1999.

[3] X. B. Nguyen, T. Komatsuzaki, and H. T. Truong, "Adaptive parameter identification of Bouc-wen hysteresis model for a vibration system using magnetorheological elastomer," *International Journal of Mechanical Sciences*, vol. 213, Article ID 106848, 2022.

[4] Y. Q. Guo, J. Zhang, D. Q. He, and J. B. Li, "Magnetorheological elastomer precision platform control using OFFO-pid algorithm," *Advances in Materials Science and Engineering*, vol. 2020, Article ID 3025863, 9 pages, 2020.

[5] G. J. Liao, X.-L. Gong, S. H. Xuan, C. J. Kang, and L. H. Zong, "Development of a real-time tunable stiffness and damping vibration isolator based on magnetorheological elastomer," *Journal of Intelligent Material Systems and Structures*, vol. 23, no. 1, pp. 25–33, 2011.

[6] X. B. Nguyen, T. Komatsuzaki, and N. Zhang, "A nonlinear magnetorheological elastomer model based on fractional viscoelasticity, magnetic dipole interactions, and adaptive smooth Coulomb friction," *Mechanical Systems and Signal Processing*, vol. 141, 2020.

[7] Y. Yu, A. N. Hoshyar, H. Li, G. Zhang, and W. Wang, "Nonlinear characterization of magnetorheological elastomer-based smart device for structural seismic mitigation," *International Journal of Social Network Mining*, vol. 139 pages, 2021.

[8] Y. Yu, Y. Li, J. Li, X. Gu, and S. Royel, "Nonlinear characterization of the MRE isolator using binary-coded discrete CSO and ELM," *International Journal of Structural Stability and Dynamics*, vol. 18, no. 08, p. 24, Article ID 1840007, 2018.

[9] Y. Yu, S. Royel, J. Li, Y. Li, and Q. Ha, "Magnetorheological elastomer base isolator for earthquake response mitigation on building structures: modeling and second-order sliding mode control," *Earthquakes and Structures*, vol. 11, no. 6, 2016.

[10] H. Madani, M. Kooshafar, and M. Emadi, "Compressive strength prediction of nanosilica-incorporated cement mixtures using adaptive neuro-fuzzy inference system and artificial neural network models," *Practice Periodical on Structural Design and Construction*, vol. 25, no. 3, August 2020.

[11] X. B. Nguyen, T. Komatsuzaki, Y. Iwata, and H. Asanuma, "Fuzzy semiactive vibration control of structures using magnetorheological elastomer," *Shock and Vibration*, Hindawi, vol. 2017, 15 pages, 2017.

[12] L. M. Jansen and S. J. Dyke, "Semiactive control strategies for MR dampers: comparative study," *Journal of Engineering Mechanics*, vol. 126, no. 8, pp. 795–803, 2000.

[13] Y. Wang and S. Dyke, "Modal-based LQG for smart base isolation system design in seismic response control," *Structural Control and Health Monitoring*, vol. 20, no. 5, pp. 753–768, 2013.

[14] M. D. Symans and S. W. Kelly, "Fuzzy logic control of bridge structures using intelligent semi-active seismic isolation systems," *Earthquake Engineering & Structural Dynamics*, vol. 28, no. 1, pp. 37–60, 1999.

[15] X. B. Nguyen, T. Komatsuzaki, Y. Iwata, and H. Asanuma, "Modeling and semi-active fuzzy control of magnetorheological elastomer-based isolator for seismic response reduction," *Mechanical Systems and Signal Processing*, vol. 101, pp. 449–466, 2018.

[16] J. Fei and M. Xin, "Robust adaptive sliding mode controller for semi-active vehicle suspension system," *International Journal of Innovative Computing, Information and Control*, vol. 8, no. 1B, pp. 691–700, 2012.

[17] Z. Chen and H. Lu, "Optimal semiactive damping control for a nonlinear energy sink used to stabilize milling," *Shock and Vibration*, vol. 2020, pp. 1–11, Article ID 8837753, 2020.

[18] X. B. Nguyen, T. Komatsuzaki, Y. Iwata, and H. Asanuma, "Robust adaptive controller for semi-active control of uncertain structures using a magnetorheological elastomer-based isolator," *Journal of Sound and Vibration*, ScienceDirect, vol. 434, , pp. 192–212, 2018.

[19] S. Liu, R. Hao, D. Zhao, and Z. Tian, "Adaptive dynamic surface control for active suspension with electro-hydraulic actuator parameter uncertainty and external disturbance," *IEEE Access*, vol. 8, pp. 156645–156653, 2020.

[20] W. Sun, H. Gao, and O. Kaynak, "Vibration isolation for active suspensions with performance constraints and actuator saturation," *IEEE*, vol. 20, no. 2, pp. 675–683, April 2015.

[21] M. U. Saeed, Z. Sun, and S. Elias, "Research developments in adaptive intelligent vibration control of smart civil structures," *Journal of Low Frequency Noise, Vibration and Active Control*, vol. 138 pages, 2021.

[22] Y. Zhang, Y. Liu, and L. Liu, "Minimal learning parameters-based adaptive neural control for vehicle active suspensions with input saturation," *Neurocomputing*, vol. 396, pp. 153–161, 2019.

[23] Z. Rashid, M. Tantray, and E. N. Farsangi, "Acceleration response-based adaptive strategy for vibration control and location optimization of magnetorheological dampers in multistoried structures," *Practice Periodical on Structural Design and Construction*, vol. 27, no. 1, February 2022.

[24] W. He, Y. Dong, and C. Sun, "Adaptive neural impedance control of a robotic manipulator with input saturation," *IEEE Transactions on Systems, Man, and Cybernetics: Systems*, vol. 46, no. 3, pp. 334–344, 2016.

[25] G. Li and Z. B. Yang, "Modelling and analysis of a magnetorheological damper with nonmagnetized passages in piston and minor losses," *Shock and Vibration*, vol. 2020, Article ID 2052140, 12 pages, 2020.

[26] X. Yuan, T. Tian, H. Ling, T. Qiu, and H. He, "A review on structural development of magnetorheological fluid damper," *Shock and Vibration*, vol. 2019, Article ID 1498962, 33 pages, 2019.

[27] J. Yang, H. Du, W. Li et al., "Experimental study and modeling of a novel magnetorheological elastomer isolator," *Smart Materials and Structures*, vol. 22, no. 11, Article ID 117001, 2013.

[28] X. Gu, J. Li, and Y. Li, "Experimental realisation of the real-time controlled smart magnetorheological elastomer seismic isolation system with shake table," *Structural Control and Health Monitoring*, vol. 27, no. 1, Article ID e2476, 2020.

[29] X. Gu, Y. Yu, J. Li, and Y. Li, "Semi-active control of magnetorheological elastomer base isolation system utilising learning-based inverse model," *Journal of Sound and Vibration*, vol. 406, pp. 346–362, 2017.

[30] M. M. Polycarpou, "Stable adaptive neural control scheme for nonlinear systems," *IEEE Transactions on Automatic Control*, vol. 41, no. 3, pp. 447–451, 1996.

[31] J. Ming and Y. M. Chen, "A smooth switching adaptive controller for linearizable systems with improved transient performance," *International Journal of Adaptive Control and Signal Processing*, vol. 20, no. 9, pp. 431–446, 2006.

[32] X. B. Nguyen, T. Komatsuzaki, and H. T. Truong, "Novel semiactive suspension using a magnetorheological elastomer (MRE)-based absorber and adaptive neural network controller for systems with input constraints," *Mechanical Sciences*, vol. 11, no. 2, pp. 465–479, 2020.